Wolframite-type MnMoO4: Magnetization, sintering by Cool-SPS, and magnetodielectric effect

Christophe Payen, Thomas Hérisson de Beauvoir, Philippe Deniard, Stéphane Jobic, U-Chan Chung, Dominique Michau, Michaël Josse

Ceramics International xxx (xxxx) xxx

Contents lists available at ScienceDirect

Ceramics International

journal homepage: www.elsevier.com/locate/ceramint

Wolframite-type $MnMoO_4$: Magnetization, sintering by Cool-SPS, and magnetodielectric effect

Christophe Payen [a,*], Thomas Hérisson de Beauvoir [b], Philippe Deniard [a], Stéphane Jobic [a], U-Chan Chung [b], Dominique Michau [b], Michaël Josse [b,**]

[a] Nantes Université, CNRS, Institut des Matériaux de Nantes Jean Rouxel, IMN, F-44000, Nantes, France
[b] Univ. Bordeaux, CNRS, Bordeaux INP, ICMCB, UMR 5026, F-33600, Pessac, France

ARTICLE INFO

Keywords:
$MnMoO_4$
Low temperature sintering
Cool-SPS
Magnetic properties
Dielectric properties

ABSTRACT

Dense ceramic samples of wolframite-type $MnMoO_4$ (*w*-$MnMoO_4$) have been prepared by Cool-SPS (Spark Plasma Sintering) for the first time with the goal of investigating the magnetic, dielectric, and magneto-electric properties of this thermally fragile polymorph of $MnMoO_4$. Earlier studies found that *w*-$MnMoO_4$ converts to the structurally different α-$MnMoO_4$ phase if heated in air at 873 K, thus hindering fabrication of *w*-$MnMoO_4$ ceramics by conventional high-temperature sintering. Unsintered powder samples, which were prepared via a hydrothermal method, and dense ceramics elaborated by Cool-SPS have the same magnetic properties. Magnetic susceptibilities display Curie-Weiss behaviour, $\chi = C/(T-\theta)$, with effective moments for Mn^{2+} ion $\mu_{eff} \approx 5.9\ \mu_B$/Mn-atom and negative Weiss temperatures $\theta \approx$ - 96 to - 98 K. Unlike the isostructural multiferroic compounds $MnW_{1-x}Mo_xO_4$ ($0 \leq x < 0.3$) which exhibits at least two successive magnetic transitions below 15 K, *w*-$MnMoO_4$ undergoes only one paramagnetic-to-antiferromagnetic transition at $T_N \approx 32$ K. The field-dependent magnetization at 2 K shows a spin-flop transition at $\mu_0 H_{SF} \approx 2$ T. Capacitance and dielectric losses obtained for a ceramic between 2 and 300 K in zero field and in a field of 9 T reveal several weak anomalies. Dielectric anomalies are observed at the magnetic phase transition, suggesting a magnetoelectric coupling. Qualitatively different dielectric and magnetodielectric behaviours occur in α-$MnMoO_4$ ceramics at low temperature.

1. Introduction

Transition metal molybdates of the $MMoO_4$ type where M is Mn, Fe, Co, Ni, or Zn have attracted great interest because of their interesting physical properties and their potential applications in several fields, including catalysis [1,2], energy storage materials [3,4], and color pigments [5]. Among these compounds, α-$MnMoO_4$, the polymorph of $MnMoO_4$ stable under ambient conditions of temperature and pressure, has been well studied for its interesting magnetic [6–11], dielectric [12, 13], electrochemical [14–17], and catalytic properties [18,19]. Its monoclinic (S.G. *C2/m*) crystal structure contains clusters of edge-sharing MnO_6 octahedra and MoO_4 tetrahedra [20] (Fig. S1).

The present study is mainly concerned with another less-studied polymorh of $MnMoO_4$, hereinafter termed w-$MnMoO_4$, which adopts the wolframite (monoclinic, S.G. *P2/c*) crystal structure [21–23]. This structure comprises zigzag $(MnO_4)_\infty$ and $(MoO_4)_\infty$ chains, running parallel to the same direction, of either edge-sharing MnO_6 distorted octahedra or edge-sharing MoO_6 distorted octahedra [23] (Fig. S1). Like in α-$MnMoO_4$, w-$MnMoO_4$ contains magnetic Mn^{2+} ions and nonmagnetic Mo^{6+} ions. w-$MnMoO_4$ can be prepared in polycrystalline form by high-pressure high-temperature solid state reaction method or by hydrothermal synthesis [21–25]. w-$MnMoO_4$ converts to the alpha form upon heating in air at 873 K [21,25]. It is worth noting that w-$MnMoO_4$ is isostructural with $MnWO_4$, which is a well-known magnetoelectric multiferroic [26–28]. $MnWO_4$ displays unusual magnetic properties that result from competing, i.e. frustrated, spin-exchange interactions [29, 30]. Three antiferromagnetic (AF) structures have been observed at low temperatures below $T_N = 13.5$ K, $T_2 = 12.5$ K and $T_1 \approx 8$ K [29], one of these magnetic phases being ferroelectric. Multiferroïcity has been actually observed below $T_2 = 12.5$ K on single-crystals [26–28], polycrystalline samples [31], and even nanostructured ceramics with average grain size of ≈50 nm [32]. In spite of its structural similarity

* Corresponding author.
** Corresponding author.
E-mail addresses: christophe.payen@cnrs-imn.fr (C. Payen), michael.josse@u-bordeaux.fr (M. Josse).

https://doi.org/10.1016/j.ceramint.2023.12.188
Received 27 October 2023; Received in revised form 7 December 2023; Accepted 13 December 2023
Available online 17 December 2023

with $MnWO_4$, w-$MnMoO_4$ has been far less studied than the α polymorph. Existing results on w-$MnMoO_4$ include a DFT (density functional theory) investigation [33] and IR and Raman data [24,25]. To the best of our knowledge, no magnetic or dielectric data have been reported so far. Herein, we report on magnetization data for powders and for dense ceramics prepared by spark plasma sintering (SPS) at temperature T < 773 K ("Cool-SPS" [34]). The Cool-SPS process made it possible to avoid the temperature-driven phase transformation of w-$MnMoO_4$ into α-$MnMoO_4$. The fabrication of dense w-$MnMoO_4$ ceramics allowed us to conduct dielectric measurements below 300 K in zero magnetic field or in a magnetic field of 9 T. Dielectric data were also collected for α-$MnMoO_4$ ceramics that were also prepared by Cool-SPS.

2. Materials and methods

2.1. Synthesis of powders and Cool-SPS sintering

w-$MnMoO_4$ powders were synthetized using the two-step method described by Clearfield et al. [23]. All high-purity reagents were purchased from commercial vendors. $MnMoO_4.H_2O$ precursor was first prepared by precipitation in aqueous solution. 100 mL of a 1 M $MnSO_4.H_2O$ aqueous solution was added slowly to 100 mL of a 1 M $Na_2MoO_4.2H_2O$ aqueous solution under stirring. The slurry was refluxed for 2 days. After filtration, the $MnMoO_4.H_2O$ precipitate was washed and dried in air. Anhydrous w-$MnWO_4$ polycrystalline samples were then obtained after hydrothermal reaction of $MnMoO_4.H_2O$ with $Na_2MoO_4.2H_2O$ in a Teflon-lined autoclave for 3 days at 473 K. The autoclave was then slowly cooled to room temperature. The product was washed with water and ethanol and dried in air.

w-$MnMoO_4$ and α-$MnMoO_4$ ceramics were prepared by Cool-SPS using a Dr. Sinter system (Model SPS-511S/SPS-515S) in a WC:Co 6 mm die using 0.16–0.18 g of hydrothermally synthesized w-$MnMoO_4$ powder for each sintering attempt. Graphite foils were used to separate the sample from the die. A K-type thermocouple was used to monitor temperature. Sintering attempts were performed under primary vacuum of about 10 Pa. Densification was monitored through the displacement of a punch rod.

2.2. Characterization

Scanning electron microcopy (SEM) and Energy Dispersive X-ray (EDX) analyses were performed at different positions of the sample surfaces. X-ray diffraction (XRD) patterns were collected at room temperature on a Bruker D8 Advance instrument using monochromatic $Cu_{K\text{-}L3}$ (λ = 1.540598 Å) X-rays and a LynxEye detector, in the 8–100° 2θ range using 0.011° steps and an acquisition time of 1.6 s per step. For the SPS sintered samples, XRD patterns were recorded on unground disks on the same equipment in the 10–100° 2θ range with 0.008° steps of 1.8 s each. Rietveld analyses of the XRD data were performed using JANA 2006 and the Cheary-Coelho fundamental approach for XRD profile parameters [35,36]. Differential scanning calorimetry and thermogravimetric analyses (DSC/TGA) measurements were performed on undensified powder samples in flowing air. Samples were heated up to 1423 K at 2 K/min, and the resulting powders were analyzed by XRD. Additional DSC measurements were taken in air below room-temperature in the 173–300 K temperature range. DC magnetization data were collected using a Quantum Design MPMS-XL7 magnetometer. Zero-field-cooled (ZFC) and field-cooled (FC) measurements were taken on warming the samples from 2 to 300 K in an applied magnetic field of $H = 1000$ Oe ($\mu_0 H = 0.1$ T). ZFC and FC datasets were found to overlap. Therefore, only ZFC measurements will be presented hereafter. Isothermal magnetization $M(H)$ curves were linear up to at least $\mu_0 H \approx 2$ T both at 2 K and 300 K. Thus the temperature-dependent susceptibility could be defined as the ratio of the magnetization measured at 1000 Oe to the applied field, $\chi = M/H$. We wrapped the powder samples in plastic films so that they had the same geometry than that of the ceramic disk. Dielectric properties of ceramics were studied using a Quantum Design Physical Properties Measurement System (PPMS), which can operate in the ranges 2–400 K and 0–9 T. To ensure electric contact, $MnMoO_4$ (w- and α-forms) ceramics were equipped with silver electrodes on both faces (planar capacitor geometry) and silver wires were subsequently added. The dielectric measurements were carried out in the frequency range of 1 kHz-1Mhz, with an applied ac electric field of 1 V, using an HP4194a impedance bridge. Capacitance and dielectric losses were measured continuously while the sample was heated and cooled at rates of 1 K/min. In the absence of significant differences, only the data collected on heating are presented here, while for sake of clarity, single-frequency plots are provided.

3. Results and discussion

3.1. Characterization of undensified polycrystalline samples of w-$MnMoO_4$

EDX elemental analyses showed no evidence for incorporation of sodium cations. Mn/Mo atomic ratio were found to be equal to 1 within the uncertainty. Volumetric mass density (ρ) measurements performed at room temperature yielded ρ = 5.2 g/cm^3, in very good agreement with the values calculated using the cell parameters derived from X-ray diffraction data (see below). As can be seen in the SEM image shown in

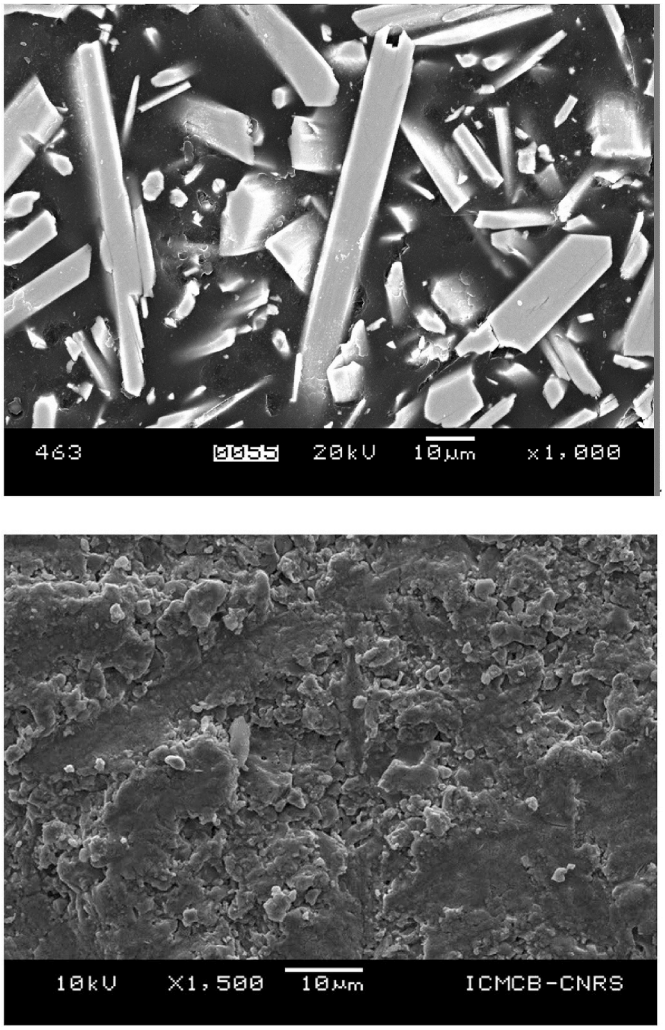

Fig. 1. SEM images of representative samples of *w*-$MnMoO_4$. Top: Polished section of a polycrystalline sample prepared via the hydrothermal method. Bottom: SPS ceramic obtained after sintering at 753 K and 500 MPa.

Fig. 1, our samples consist mainly of needle-shaped microcrystals. Fig. 2 displays the room temperature XRD pattern. All reflections could be indexed using the PDF card # 78–0221, which was obtained from single-crystal data for w-$MnMoO_4$ (ICSD # 61,078). However, the relative intensities of several reflections differ strongly from those of the PDF card. In view of the microcrystal morphologies, these discrepancies in relative intensities likely indicates that every possible crystalline orientation is not represented equally in the sample. Despite this, we attempted to perform a Rietveld refinement using the published monoclinic *P2/c* structural model for w-$MnMoO_4$ [23] and a March-Dollase function [37, 38] in order to take into account preferred orientation along the [100] direction. The refinement converged to the results shown in Fig. 2. As can be seen in this figure, there are discrepancies between observed and calculated intensities for a few reflections, and this cannot be ascribed to the signal-to-noise ratio. These discrepancies are due to the large crystallite size and to the morphology of the microcrystals. The refined crystallite size and microstrain parameter are 545 (28) nm and 10.8 (4) %, respectively. Cell parameters, agreement factors and atomic parameters are gathered in Table S1. Cell parameters (a = 4.82146 (8) Å, b = 5.75626 (16) Å, c = 4.9656 (2) Å, and β = 90.8463 (18)) and atom positions are consistent with those earlier reported for a single-crystal prepared via the same hydrothermal route [23].

DSC/TGA measurements are shown in Fig. S2. An exothermic process occurs just above 773 K with no significant change of mass. The post-DSC products were analyzed by XRD, and they consist of phase-pure α-$MnMoO_4$. These results are consistent with two earlier works that reported complete transformation of the wolframite form into the alpha form at 873 K [21,25]. However, to the best of our knowledge, no DCS data have been reported so far.

3.2. Sintering by Cool-SPS and characterization of ceramics

Preliminary experiments revealed that w-$MnMoO_4$ converts to α-$MnMoO_4$ around 773 K in Cool-SPS conditions. This is comparable with the temperature range of 773–873 K for this conversion, as observed from thermal characterizations (Fig. S2). In addition, densification takes place around 753 K, leaving an extremely small thermal window for the sintering of w-$MnMoO_4$ ceramics. Optimal sintering conditions were found to be a 500 MPa pressure and 753 K temperature with 10 min dwell time. These conditions yield either phase-pure w-$MnMoO_4$ ceramics or α-$MnMoO_4$ containing ceramics, according to XRD data. This difficulty in monitoring the densification is due to the very small thermal window available for sintering without conversion from w-to α-$MnMoO_4$. The actual sample conditions may then slightly depart from the target ones, due to thermocouple and sample positioning, die mounting, etc. Among the best w-$MnMoO_4$ ceramics obtained in these conditions (phase-pure, relative density of 90% and above) one was used to check the microstructure by SEM, while another one was kept for further physical characterization (XRD, magnetization and dielectric measurements). As can be seen in Fig. 1, SEM micrographs display features consistent with a 90% densified sample, and show no trace of the acicular microcrystals used as the starting material, which is likely due to grain growth under Cool-SPS conditions promoting a different growth pattern. The room temperature XRD pattern of a w-$MnMoO_4$ ceramic disk, which was later used for magnetic and dielectric measurements, is displayed in Fig. 3. Note that randomness of the crystallite orientation is most probably not achieved for the pellet produced at 500 MPa. Like in undensified samples, however, Rietveld refinement was conducted using the published monoclinic *P2/c* structural model for w-$MnMoO_4$ and a March-Dollase function to take into account preferred orientation while fitting. Refinements results are gathered in Table S2. Reflections are broader than those observed in the undensified powder not only because of a larger microstrain parameter of 56 (2) % but also because of a smaller crystallite size of 141 (9) nm. As for the undensified polycrystalline samples, cell parameters and atom positions agree well with published data for a single-crystal [23].

3.3. Magnetization of powders and ceramics

Fig. 4 shows the inverse molar magnetic susceptibilities, $1/\chi(T)$, obtained for a powder sample and for a dense w-$MnMoO_4$ ceramic between 2 and 300 K. As anticipated from the XRD results, samples in a powder form and the ceramic disk have the same behavior. In the high temperature range, the magnetic susceptibilities follow Curie-Weiss behaviors, $\chi(T) = C/(T-\theta)$. The calculated effective magnetic moments, $\mu_{eff} = 5.9\ \mu_B$/f.u., are consistent with high-spin Mn^{2+} (d^5, $S = 5/2$) and nonmagnetic Mo^{6+} ions. Weiss temperatures θ lie in the range of −96 to −98 K, indicating dominant AF interactions. As can be seen in Fig. 5, a maximum occurs in the susceptibility versus temperature curve at T (χ_{max}) = 34 K. The onset of magnetic order is observed close to this maximum at T_N = 32 K, as determined from the d (χ.T)/dT versus T curve (Fig. 5). The small T (χ_{max})/T_N ratio and the absence of a broad maximum in $\chi(T)$ above T_N indicate that w-$MnMoO_4$ behaves as a three dimensional (3D) antiferromagnet [39]. Furthermore, the behavior of $\chi(T)$ below T_N is consistent with a collinear antiferromagnetic structure. For a uniaxial two-sublattice antiferromagnet, the susceptibility of a polycrystalline sample at temperatures well below T_N is expected to be

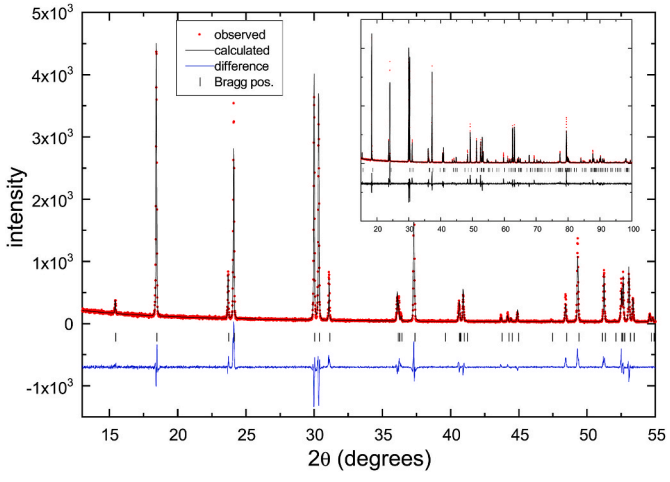

Fig. 2. (color) A portion of the final Rietveld refinement plots of the room-temperature XRD data (taken with $Cu_{K\text{-}L3}$ radiation) for an undensified polycrystalline sample of w-$MnMoO_4$. Insert shows the full pattern.

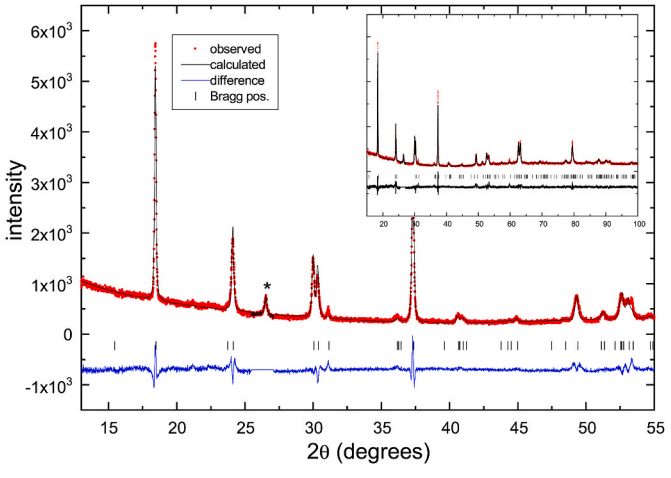

Fig. 3. (color) A portion of the final Rietveld refinement plots of the room-temperature XRD data (taken with $Cu_{K\text{-}L3}$ radiation) for a ceramic disk of *w*-$MnWO_4$. The star denotes a reflection due to the graphite foil used during the SPS process (PDF # 26–1076). Insert shows the full pattern.

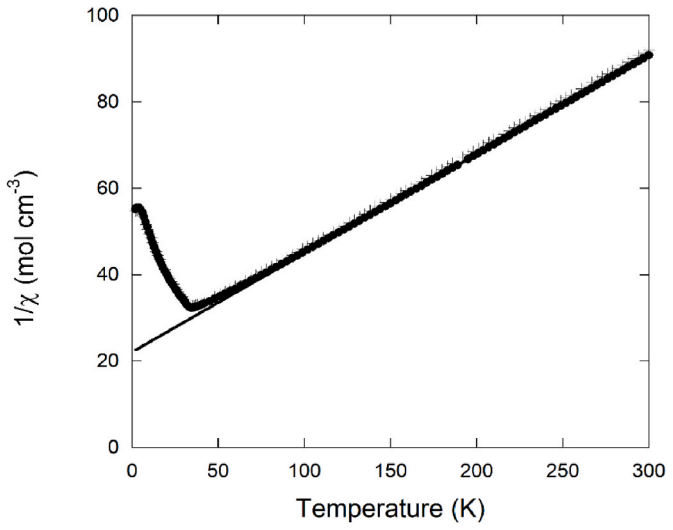

Fig. 4. Inverse molar magnetic susceptibility $1/\chi$ versus temperature T for a powder sample (black circles) and for a dense ceramic of w-$MnMoO_4$ (plus signs). The solid line corresponds to Curie-Weiss behaviour for the powder, $1/\chi = (T-\theta)/C$, with $C = 4.38$ cm^3 K mol^{-1} and $\theta = -96$ K obtained by fitting the data in the temperature range of 200–300 K.

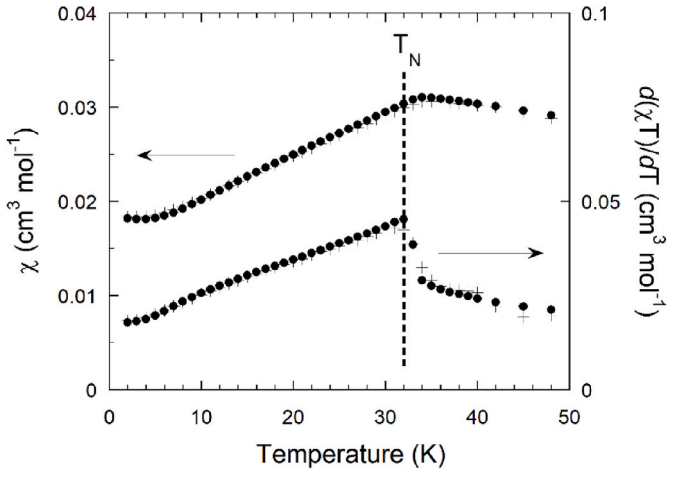

Fig. 5. Magnetic susceptibility $\chi(T)$ at low temperatures (left vertical axis) for a powder sample (black circles) and for a ceramic sample of w-$MnMoO_4$ (plus signs). The vertical dashed line indicates the transition temperature $T_N = 32$ (1) K, as determined from the d (χ.T)/dT versus T curve (right vertical axis).

nearly 2/3 its value at T_N [40]. Fig. 6 shows the 2 K isothermal magnetization scan, $M(H)$, recorded up to $\mu_0 H = 7$ T. At low field, the anticipated linear AF response is observed up $\mu_0 H \approx 2$ T. For higher field strengths, the observed deviation from the low-field linear behavior is typical for a spin-flop. Spin-flop transitions can be observed in antiferromagnets with small magnetic anisotropies when the magnetic field is applied parallel to the preferred axis of spin alignment [39]. A small magnetic anisotropy is indeed expected for high-spin Mn^{2+} because this ion has an orbitally nondegenerate $^6A_{1g}$ ground state irrespective of the symmetry of the crystal field [40,41]. The 2 K isothermal magnetization is far from being saturated at 7 T, in agreement with the high value of the absolute Weiss temperature θ. The value of the magnetization at 7 T ($\approx$2200 emu mol^{-1}) is actually much less than the expected saturation magnetization g.S.$\mu_B = 5$ μ_B/Mn-atom or 27,925 emu mol^{-1} for g = 2.

We can now compare the results of our initial magnetization study of w-$MnMoO_4$ with earlier works on α-$MnMoO_4$ [6–11] and on the wolframite-type $MnW_{1-x}Mo_xO_4$ ($0 \leq x < 0.3$) solid solution [42,43]. The

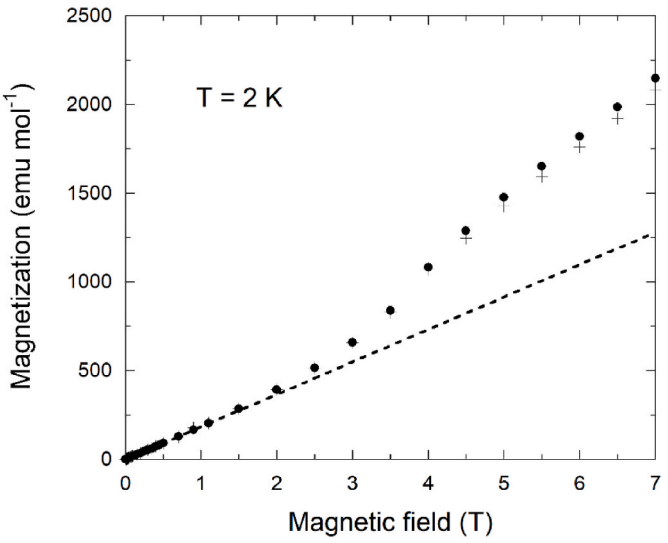

Fig. 6. Magnetic field dependence of magnetization measured at 2 K for a powder sample (black circles) and for a dense ceramic sample of w-$MnMoO_4$ (plus signs). The dashed line indicates the linear increase of the magnetization for magnetic field smaller than 2 T.

absolute Weiss temperature $|\theta|$ and the Néel transition temperature T_N in w-$MnMoO_4$ are higher than those observed both in α-$MnMoO_4$ and $MnWO_4$. In α-$MnMoO_4$, magnetic couplings between Mn^{2+} ions lead to a negative Weiss temperature $\theta = -33$ K and to a Néel temperature $T_N = 11$ K [6–8]. Field-dependence magnetization data taken at 2 K for α-$MnMoO_4$ reveal a spin-flop transition at $H_{SF} = 2.9$ T and show no sign of saturation for magnetic fields up to 12 T [11]. In $MnWO_4$, $\theta = -71$ K and three magnetic transitions are observed at $T_N = 13.5$ K, $T_2 = 12.3$ K, and $T_1 = 7.5$ K [29]. A magnetically induced ferroelectricity is observed between T_1 and T_2 [26–28]. The spin-spiral magnetic order between T_1 and T_2 has incommensurate components in the a and c axis, which reflects magnetic frustration in these two directions [29]. In wolframite $MnW_{1-x}Mo_xO_4$ solid solution ($0 \leq x < 0.3$), $|\theta|$, the magnetic transition temperatures T_N and T_2, and the ferroelectric transition temperature T_2 all slightly increases with the Mo content due to doping-induced increase in the overall magnetic interaction, which is itself the result of doping-induced tuning of the orbital hybridization between Mn 3d and O 2p states [42,43]. For $x < 0.3$, T_N increases with Mo content at a rate of 0.063 K per 1 mol % Mo. By extrapolating to $x = 1$, a T_N value of about 20 K, which is lower than the observed one, is calculated for w-$MnMoO_4$. A DFT analysis of nine spin-exchange interactions between Mn^{2+} ions of $MnWO_4$ and of w-$MnMoO_4$ suggested that the substitution of Mo^{6+} for W^{6+} strengthens the overall magnetic interaction indeed [42]. While exchange couplings in $MnWO_4$ are all AF, the DFT analysis also revealed sign reversal, from AF to F, of three spin-exchange parameters in w-$MnMoO_4$. These sign changes of couplings should suppress magnetic frustration and hence both the spin-spiral magnetic order and its associated ferroelectricity. This most likely explain why, unlike in $MnW_{1-x}Mo_xO_4$ ($0 \leq x < 0.3$), w-$MnMoO_4$ exhibits only one magnetic transition.

3.4. Dielectric properties of ceramics

Fig. 7 shows the temperature dependences of the capacitance and dielectric losses measured in zero magnetic field or in a field of 9 T for a w-$MnMoO_4$ ceramic. Three dielectric anomalies, marked with (1), (2), and (3) in Fig. 7, can be identified. They all are very small in amplitude. The first one (1) appears in the capacitance, without significant modification of losses. This step-like anomaly is associated with magnetic ordering in the sample, as it occurs at T_N (32 K). Upon application of a 9 T magnetic field, this anomaly is still present, but appears less marked.

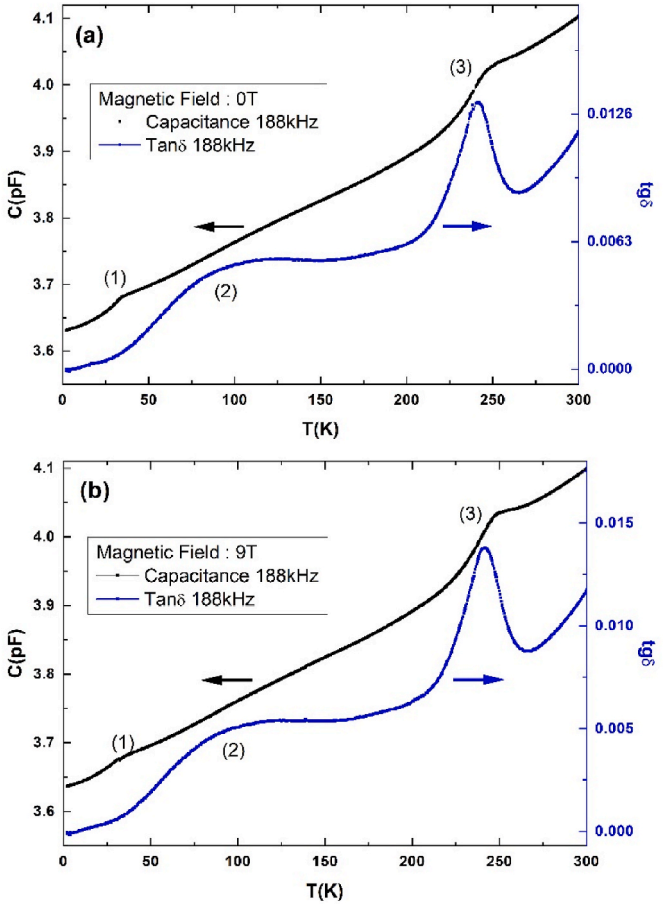

Fig. 7. (color) Capacitance (black curves), *C*, and dielectric losses (blue curves), *tgδ*, plotted as a function of temperature, *T*, measured at 188 kHZ **(a)** in zero magnetic field or **(b)** in a field of 9 T for a w-$MnMoO_4$ ceramic.

The second anomaly (2) is clearly visible in the dielectric losses, as a broad hump centered around 100 K, and is associated with a frequency dependence of the capacitance, i.e. a dielectric dispersion in the capacitance (not visible in Fig. 7 since a single frequency is plotted for the sake of clarity; see Fig. S3). It is thus the signature of a relaxation of small amplitude, which origin could be electronic, since the dielectric dispersion closes at T_N (Fig. S3). This second dielectric anomaly seems unaffected by the application of a 9 T magnetic field. The third anomaly (3) peaks around 240 K and displays signatures in both capacitance and dielectric losses, suggesting it could be related to a minor structural modification (rotation of polyhedra, minor rearrangement of coordination spheres …). Both the temperature dependent magnetization measured at 0.1 T (Fig. 4) and our DSC data collected from room temperature down to 173 K (not shown) showed no corresponding anomaly around 240 K. This third dielectric anomaly is qualitatively unaffected by the application of a 9 T magnetic field.

It is of interest to focus on the dielectric anomaly (1) associated with the antiferromagnetic ordering at T_N. As can be seen in Fig. 8, the capacitance displays a different behaviour around T_N with respect to the magnetic field. The shape of the dielectric anomaly at T_N under 9 T is different from the step-like anomaly observed without magnetic field. Actually, instead of the zero-field capacitance decreasing more rapidly with decreasing temperature, the capacitance measured at 9 T increases first, before resuming a temperature dependence identical to that observed under 0 T, as confirmed by plotting a dataset normalized at 2 K (see Fig. S4). This results in a larger capacitance under a magnetic field of 9 T (Fig. 8), and thus, at least, a magnetodielectric effect ($\varepsilon = f(H)$). The amplitude of this effect is around 0.2%, and it could be related to the

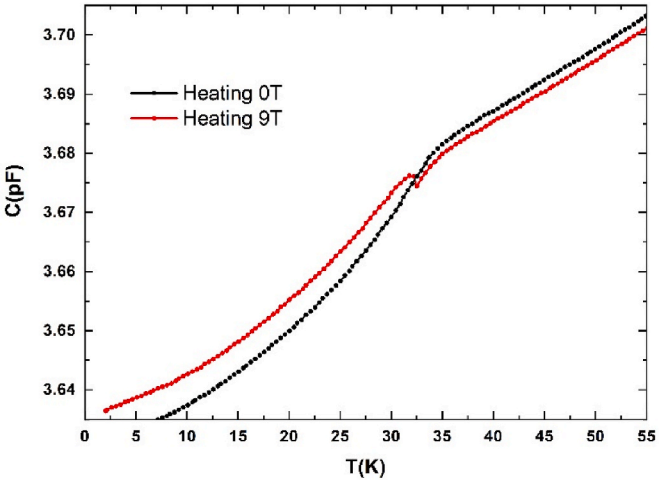

Fig. 8. (color) Temperature-dependent capacitance *C(T)* of a w-$MnMoO_4$ ceramic measured at 188 kHz in zero magnetic field (black curve, "0 T") or in an applied magnetic field of 9 T (red curve, "9T"), plotted for temperatures lower than 55 K.

spin-flop transition observed from magnetic measurements for magnetic fields exceeding 2 T.

These findings are of great interest, especially when compared with the dielectric behaviour of a ceramic of α-$MnMO_4$ prepared by Cool-SPS as well. To the best of our knowledge, no low-temperature dielectric data have been reported on for α-$MnMoO_4$ so far. As can be seen in Fig. 9, a monotonous decrease of the capacitance is observed when cooling down the α-$MnMoO_4$ ceramic to around 11 K. Below 11 K, i.e. below the Néel temperature of α-$MnMoO_4$, the capacitance increases without displaying any signature ascribable to a dielectric transition. Applying a magnetic field of 9 T to this α-$MnMoO_4$ ceramic diminishes the capacitance, while it increases below ≈30 K under 9 T in w-$MnMoO_4$, showing that different dielectric and magnetodieletric effects occur around the magnetic transitions in these polymorphs.

For both α and w polymorphs, our temperature-dependent dielectric data were acquired under an applied magnetic field (9 T) higher than the spin-flop field but lower than the saturation field (see section 3.3). Therefore, those crystallites for which the magnetic easy axis is roughly

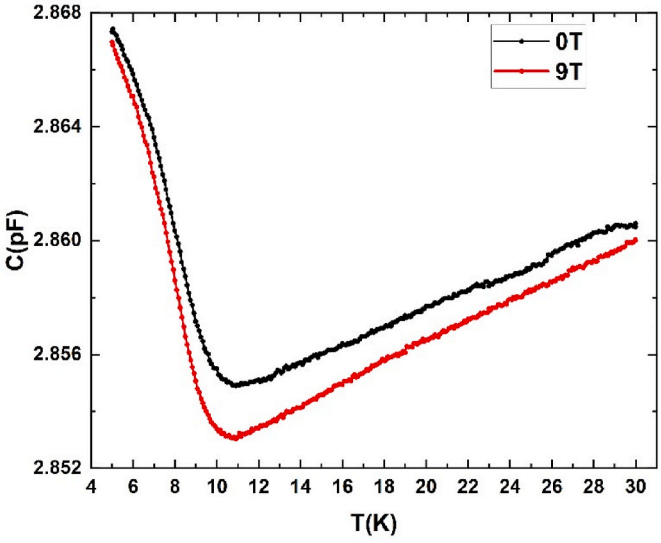

Fig. 9. (color) Temperature-dependent capacitance *C(T)* of an α-$MnMoO_4$ ceramic measured at 188 kHz in zero magnetic field (black curve, "0T") or in an applied magnetic field of 9 T (red curve, "9T").

parallel to the applied magnetic field undergo a paramagnetic to spin-flop magnetic transition at a temperature around T_N instead of the usual paramagnetic to antiferromagnetic transition at T_N [39]. The magnetic field-induced spin reorientation could well have an impact on the low-temperature dielectric behavior of α and w-$MnMoO_4$ observed at 9 T. Actually, spin-flop driven changes in the dielectric constant have been observed in some other antiferromagnets [44–47].

4. Conclusion

We have reported for the first time on the magnetic and dielectric characterization of w-$MnMoO_4$. Dense ceramics of the "thermally fragile" oxide w-$MnMoO_4$ and of α-$MnMoO_4$ as well have been obtained by Cool-SPS to conduct reliable dielectric measurements below room-temperature. Both the magnetic and dielectric behaviors of w-$MnMoO_4$ differ from those of wolframite $MnW_{1-x}Mo_xO_4$ ($0 \leq x < 0.3$) solid solution and of α-$MnMoO_4$. Magnetization data have indicated that w-$MnMoO_4$ behaves as a three-dimensional antiferromagnet with a Néel temperature of 32 K and have suggested a spin-flop transition. Unlike in wolframite $MnW_{1-x}Mo_xO_4$ solid solution, there is no evidence for a ferroelectric transition and hence for multiferroicity in w-$MnMoO_4$. Yet, the dielectric anomalies seen around T_N in zero and in a 9 T magnetic field point to an interplay of dielectric and magnetic properties, presumably through the spin-flop state. The observed magnetodielectric effects at low temperature are a likely evidence of a magnetoelectric coupling.

Declaration of competing interest

The authors declare that they have no known competing financial interests or personal relationships that could have appeared to influence the work reported in this paper.

Acknowledgements

We thank Sabrina Salmon, Stéphane Grolleau, and Rodolphe Decourt for experimental assistance, Catherine Guillot-Deudon, Pascaline Patureau, Rémi Dessapt, Octavio Pena, and Mario Maglione for useful discussions, advice, and assistance with characterization.

Appendix A. Supplementary data

Supplementary data to this article can be found online at https://doi.org/10.1016/j.ceramint.2023.12.188.

References

[1] S.K. Ray, J. Hur, A review on monoclinic metal molybdate photocatalyst for environmental remediation, J. Ind. Eng. Chem. 101 (2021) 28–50, https://doi.org/10.1016/j.jiec.2021.06.027.

[2] N. Liu, R. Wu, Y. Liu, Y. Liu, P. Deng, Y. Li, Y. Du, Y. Cheng, Z. Zhuang, Z. Kang, H. Li, Oxygen vacancy engineering of Fe-doped $NiMoO_4$ for electrocatalytic N_2 fixation to NH_3, Inorg. Chem. 62 (2023) 11990–12000, https://doi.org/10.1021/acs.inorgchem.3c01467.

[3] L.-Q. Mai, F. Yang, Y.-L. Zhao, X. Xu, L. Xu, Y.-Z. Luo, Hierarchical $MnMoO_4$/$CoMoO_4$ heterostructured nanowires with enhanced supercapacitor performance, Nat. Commun. 2 (2011) 381, https://doi.org/10.1038/ncomms1387.

[4] T. Watcharatharapong, M. Minakshi Sundaram, S. Chakraborty, D. Li, G. M. Shafiullah, R.D. Aughterson, R. Ahuja, Effect of transition metal cations on stability enhancement for molybdate-based hybrid supercapacitor, ACS Appl. Mater. Interfaces 9 (2017) 17977–17991, https://doi.org/10.1021/acsami.7b03836.

[5] L. Robertson, M. Duttine, M. Gaudon, A. Demourgues, Cobalt–zinc molybdates as new blue pigments involving Co^{2+} in distorted trigonal bipyramids and octahedra, Chem. Mater. 23 (2011) 2419–2427, https://doi.org/10.1021/cm200795p.

[6] L.G. Van Uitert, R.C. Sherwood, H.J. Williams, J.J. Rubin, W.A. Bonner, Magnetic properties of a number of divalent transition metal tungstates, molybdates and titanates, J. Phys. Chem. Solid. 25 (1964) 1447–1451, https://doi.org/10.1016/0022-3697(64)90060-5.

[7] J.P. Attfield, Ferromagnetic exchange in α-manganese molybdate and the structural consequences, J. Phys. Condens. Matter 2 (1990) 6999, https://doi.org/10.1088/0953-8984/2/33/012.

[8] B. Lippold, J. Herrmann, W. Reichelt, H. Oppermann, Preparation and magnetic investigations on $MnMoO_4$ single crystals, Phys. Status Solidi A 124 (1991), https://doi.org/10.1002/pssa.2211240149. K59–K62.

[9] G. Lautenschläger, H. Weitzel, H. Fuess, The magnetic structure of α-$MnMoO_4$, Z. Für Krist. - Cryst. Mater. 209 (1994) 936–940, https://doi.org/10.1524/zkri.1994.209.12.936.

[10] S.T. Ochsenbein, G. Chaboussant, A. Sieber, H.U. Güdel, S. Janssen, A. Furrer, J. P. Attfield, Magnetic cluster excitations in the antiferromagnetic phase of $MnMoO_4$, Phys. Rev. B 68 (2003), 092410, https://doi.org/10.1103/PhysRevB.68.092410.

[11] H. Ehrenberg, B. Schwarz, H. Weitzel, Magnetic phase diagrams of α-$MnMoO_4$, J. Magn. Magn Mater. 305 (2006) 57–62, https://doi.org/10.1016/j.jmmm.2005.11.027.

[12] Y.P. Yadava, R.A. Singh, Electrical conduction in manganese molybdate, Mater. Chem. Phys. 17 (1987) 259–272, https://doi.org/10.1016/0254-0584(87)90148-9.

[13] J. Wang, Z. Qing, X. Zhou, H. Zou, H. Li, A. Liu, S. Duan, Y. Li, Crystal structure, Raman spectra, bond characteristics, and microwave dielectric properties of $MnMoO_4$ ceramics, Ceram. Int. 49 (2023) 23627–23633, https://doi.org/10.1016/j.ceramint.2023.04.197.

[14] S.-S. Kim, S. Ogura, H. Ikuta, Y. Uchimoto, M. Wakihara, Synthesis of $MnMoO_4$ as high capacity anode material for Li secondary battery, Chem. Lett. 30 (2001) 760–761, https://doi.org/10.1246/cl.2001.760.

[15] G.K. Veerasubramani, K. Krishnamoorthy, R. Sivaprakasam, S.J. Kim, Sonochemical synthesis, characterization, and electrochemical properties of $MnMoO_4$ nanorods for supercapacitor applications, Mater. Chem. Phys. 147 (2014) 836–842, https://doi.org/10.1016/j.matchemphys.2014.06.028.

[16] H. Cao, N. Wu, Y. Liu, S. Wang, W. Du, J. Liu, Facile synthesis of rod-like manganese molybdate crystallines with two-dimensional nanoflakes for supercapacitor application, Electrochim. Acta 225 (2017) 605–613, https://doi.org/10.1016/j.electacta.2017.01.021.

[17] Z. Zhu, Y. Sun, C. Li, C. Yang, L. Li, J. Zhu, S. Chou, M. Wang, D. Wang, Y. Li, Mini-review: progress on micro/nanoscale $MnMoO_4$ as an electrode material for advanced supercapacitor applications, Mater. Chem. Front. 5 (2021) 7403–7418, https://doi.org/10.1039/D1QM00914A.

[18] J. Bai, Y. Song, C. Wang, H. Chen, D. Wei, L. Bai, W. Wang, L. Yang, Y. Liang, H. Yang, Engineering the electronic structure of Mo sites in Mn–Mo–O mixed-metal oxides for efficient aerobic oxidative desulfurization, Energy Fuels 35 (2021) 12310–12318, https://doi.org/10.1021/acs.energyfuels.1c01476.

[19] L.H. da S. Lacerda, M.A. San-Miguel, DFT approaches unraveling the surface and morphological properties of $MnMoO_4$, Appl. Surf. Sci. 567 (2021), 150882, https://doi.org/10.1016/j.apsusc.2021.150882.

[20] P. Abrahams, J.M. Reddy, Crystal structure of the transition-metal molybdates. I. Paramagnetic alpha-$MnMoO_4$, J. Chem. Phys. 43 (1964) 2533–2543, https://doi.org/10.1063/1.1697153.

[21] A.P. Young, C.M. Schwartz, High-pressure synthesis of molybdates with the wolframite structure, Science 141 (1963) 348–349, https://doi.org/10.1126/science.141.3578.348.

[22] A.W. Sleight, B.L. Chamberland, Transition metal molybdates of the type AMoO4, Inorg. Chem. 7 (1968) 1672–1675, https://doi.org/10.1021/ic50066a050.

[23] A. Clearfield, A. Moini, P.R. Rudolf, Preparation and structure of manganese molybdates, Inorg. Chem. 24 (1985) 4606–4609, https://doi.org/10.1021/ic00220a035.

[24] S. Lei, K. Tang, Q. Liu, Z. Fang, Q. Yang, H. Zheng, Preparation of manganese molybdate rods and hollow olive-like spheres, J. Mater. Sci. 41 (2006) 4737–4743, https://doi.org/10.1007/s10853-006-0044-5.

[25] G.M. Martins, P.O. Coelho, K.P.F. Siqueira, R.L. Moreira, A. Dias, Investigation of polymorphism and vibrational properties of $MnMoO_4$ microcrystals prepared by a hydrothermal process, Cryst. Growth Des. 18 (2018) 2474–2485, https://doi.org/10.1021/acs.cgd.8b00102.

[26] K. Taniguchi, N. Abe, T. Takenobu, Y. Iwasa, T. Arima, Ferroelectric polarization flop in a frustrated magnet $MnWO_4$ induced by a magnetic field, Phys. Rev. Lett. 97 (2006), 097203, https://doi.org/10.1103/PhysRevLett.97.097203.

[27] A.H. Arkenbout, T.T.M. Palstra, T. Siegrist, T. Kimura, Ferroelectricity in the cycloidal spiral magnetic phase of $MnWO_4$, Phys. Rev. B 74 (2006), 184431, https://doi.org/10.1103/PhysRevB.74.184431.

[28] O. Heyer, N. Hollmann, I. Klassen, S. Jodlauk, L. Bohatý, P. Becker, J.A. Mydosh, T. Lorenz, D. Khomskii, A new multiferroic material: $MnWO_4$, J. Phys. Condens. Matter 18 (2006) L471, https://doi.org/10.1088/0953-8984/18/39/L01.

[29] G. Lautenschläger, H. Weitzel, T. Vogt, R. Hock, A. Böhm, M. Bonnet, H. Fuess, Magnetic phase transitions of $MnWO_4$ studied by the use of neutron diffraction, Phys. Rev. B 48 (1993) 6087–6098, https://doi.org/10.1103/PhysRevB.48.6087.

[30] F. Ye, R.S. Fishman, J.A. Fernandez-Baca, A.A. Podlesnyak, G. Ehlers, H.A. Mook, Y. Wang, B. Lorenz, C.W. Chu, Long-range magnetic interactions in the multiferroic antiferromagnet MnWO4, Phys. Rev. B 83 (2011), 140401, https://doi.org/10.1103/PhysRevB.83.140401.

[31] L. Meddar, M. Josse, P. Deniard, C. La, G. André, F. Damay, V. Petricek, S. Jobic, M.-H. Whangbo, M. Maglione, C. Payen, Effect of nonmagnetic substituents Mg and Zn on the phase competition in the multiferroic antiferromagnet $MnWO_4$, Chem. Mater. 21 (2009) 5203–5214, https://doi.org/10.1021/cm9021358.

[32] P. Patureau, R. Dessapt, P. Deniard, U.-C. Chung, D. Michau, M. Josse, C. Payen, M. Maglione, Persistent type-II multiferroicity in nanostructured $MnWO_4$ ceramics, Chem. Mater. 28 (2016) 7582–7585, https://doi.org/10.1021/acs.chemmater.6b03803.

[33] L.H. da S. Lacerda, M.A. San-Miguel, Unraveling the $MnMoO_4$ polymorphism: a comprehensive DFT investigation of α, β, and ω phases, J. Mater. Sci. 57 (2022) 10179–10196, https://doi.org/10.1007/s10853-022-07277-7.

[34] T.H. de Beauvoir, A. Sangregorio, I. Cornu, C. Elissalde, M. Josse, Cool-SPS: an opportunity for low temperature sintering of thermodynamically fragile materials, J. Mater. Chem. C 6 (2018) 2229–2233, https://doi.org/10.1039/C7TC05640K.

[35] V. Petricek, M. Dusek, L. Palatinus, Crystallographic computing system JANA2006: general features, Z. Kristallogr. 229 (2014) 345–352, https://doi.org/10.1515/zkri-2014-1737.

[36] R.W. Cheary, A. Coelho, A fundamental parameters approach to X-ray line-profile fitting, J. Appl. Crystallogr. 25 (1992) 109–121, https://doi.org/10.1107/S0021889891010804.

[37] A. March, Mathematische Theorie der Regelung nach der Korngestah bei affiner Deformation, Z. Für Krist. - Cryst. Mater. 81 (1932) 285–297, https://doi.org/10.1524/zkri.1932.81.1.285.

[38] W.A. Dollase, Correction of intensities for preferred orientation in powder diffractometry: application of the March model, J. Appl. Crystallogr. 19 (1986) 267–272, https://doi.org/10.1107/S0021889886089458.

[39] L.J. De Jongh, A.R. Miedema, Experiments on simple magnetic model systems, Adv. Phys. 50 (2001) 947–1170, https://doi.org/10.1080/00018730110101412.

[40] R.L. Carlin, Magnetochemistry, Springer, Berlin, Heidelberg, 1986, https://doi.org/10.1007/978-3-642-70733-9.

[41] F.E. Mabbs, D.J. Machin, Magnetism and Transition Metal Complexes, Chapman and Hall, 1973.

[42] L. Meddar, M. Josse, M. Maglione, A. Guiet, C. La, P. Deniard, R. Decourt, C. Lee, C. Tian, S. Jobic, M.-H. Whangbo, C. Payen, Increasing the phase-transition temperatures in spin-frustrated multiferroic $MnWO_4$ by Mo doping, Chem. Mater. 24 (2012) 353–360, https://doi.org/10.1021/cm2031653.

[43] V. Hardy, C. Payen, F. Damay, L. Meddar, M. Josse, G. Andre, Phase transitions and magnetic structures in $MnW_{1-x}Mo_xO_4$ compounds ($x \leqslant 0.2$), J. Phys. Condens. Matter 28 (2016), 336003, https://doi.org/10.1088/0953-8984/28/33/336003.

[44] T. Kolodiazhnyi, H. Sakurai, N. Vittayakorn, Spin-flop driven magneto-dielectric effect in $Co_4Nb_2O_9$, Appl. Phys. Lett. 99 (2011), 132906, https://doi.org/10.1063/1.3645017.

[45] L.H. Yin, Y.M. Zou, J. Yang, J.M. Dai, W.H. Song, X.B. Zhu, Y.P. Sun, Colossal magnetodielectric effect and spin flop in magnetoelectric $Co_4Nb_2O_9$ crystal, Appl. Phys. Lett. 109 (2016), 032905, https://doi.org/10.1063/1.4959086.

[46] N. Abe, N.D. Khanh, T. Sasaki, T. Arima, Magnetic-field-induced spin flop transition and magnetoelectric effect in $Ca_2Fe_{2-x}Al_xO_5$, Phys. Rev. B 89 (2014), 054437, https://doi.org/10.1103/PhysRevB.89.054437.

[47] B. Huang, J.-Y. Zhang, R.-K. Huang, M.-K. Chen, W. Xue, W.-X. Zhang, M.-H. Zeng, X.-M. Chen, Spin-reorientation-induced magnetodielectric coupling effects in two layered perovskite magnets, Chem. Sci. 9 (2018) 7413–7418, https://doi.org/10.1039/C8SC02917B.